

Generalization of the $\mu(I)$ rheology to account for flow type

Harkirat Singh^{1,*} and David Henann²

¹Mechanical and Civil Engineering, California Institute of Technology

²School of Engineering, Brown University

Abstract. Most existing rheological models for dense granular flow have been calibrated to simple shear flows, although in practice there are numerous different types of flows. One of the key ingredients of any granular rheological model is the flow threshold, i.e., the critical stress state which initiates the flow. In this study, we propose a generalized flow threshold informed by extensive discrete element simulations over a wide range of flow types. We propose a functional form for a generalized yield criterion accounting for the flow type through the third invariant (Lode-angle) of the stress deviator. Moreover, we generalize the conventional $\mu(I)$ form of local rheology to account for flow type dependence as a function of the inertial number.

1 Introduction

Granular materials have wide utility across diverse areas, such as geophysics to predict and mitigate natural hazards like landslides, pharmaceutical industry, design of military vehicles that traverse complex terrains, design of storage containers and many other applications. Predictive models for granular materials are crucial to address the aforementioned applications, but bulk granular materials display a variety of behaviors, such as segregation due to mismatches in sizes or density [1–5] or coexistence of fluid-like and solid-like regions [6] during flow. These peculiar behaviors of flowing granular media pose a challenge to predictive modeling. In the past two decades, there have been numerous efforts towards modeling rheological behavior of dense granular media [7–10].

The rheological behavior of dense granular mixtures is described by a constitutive equation relating the stresses to the deformation rates. The inertial, or $\mu(I)$ rheology [7–9, 11], where μ is the ratio of shear stress to pressure and I is the non-dimensional strain-rate (inertial number), is a common viscoplastic modeling approach for dense granular flow and uses dimensional arguments to relate the stress state to the strain rate at a point through a local constitutive equation. It states that there is a critical stress ratio μ_s , and the material flows only when $\mu > \mu_s$ and there is no flow when $\mu < \mu_s$. The $\mu(I)$ rheology has been widely used in simulating complicated scenarios such as silos flow [12], heap flow [8], and a collapsing column [13].

Despite being widely used in a variety of flows, the $\mu(I)$ rheology has traditionally been fitted only to simple shear flows. In this study, we have attempted to generalize the $\mu(I)$ rheology by accounting for the flow type in the yield criterion. The proposed yield criterion is fitted to an extensive discrete element method (DEM) dataset reported

in [14], which studies a variety of flows including irrotational flows like triaxial compression and triaxial extension. It is noted that the flow threshold varies significantly depending on the flow type. This paper is organized as follows. The useful notations and the functional form for the yield criterion is defined in sec. 2. We use the DEM data to fit the yield threshold accounting for different flow types in sec. 3. We conclude the study and list some promising future directions in sec. 4.

2 Formulation

In this section, we introduce some notations to denote the relevant continuum field variables that are used throughout this study. We use these field variables to propose a yield criterion which accounts for the flow type.

2.1 Notations

We denote the Cauchy stress as \mathbf{T} , the pressure is given as $p = -\frac{1}{3}\text{tr}\mathbf{T}$ and the stress deviator is $\mathbf{T}_0 = \mathbf{T} + p\mathbf{I}$. The second and third invariants of the stress deviator tensor can be given as $J_2 = \frac{1}{2}\mathbf{T}_0 : \mathbf{T}_0$ and $J_3 = \det\mathbf{T}_0$, respectively. The equivalent shear stress is defined as $\bar{\tau} = \frac{1}{\sqrt{2}}|\mathbf{T}_0| = \sqrt{J_2}$. The stress deviator direction tensor is given by $\mathbf{N} = \frac{\mathbf{T}_0}{|\mathbf{T}_0|} = \frac{\mathbf{T}_0}{\sqrt{2J_2}}$. Lastly, we define an alternative third invariant as $K_3 = 3\sqrt{6}\det\mathbf{N}$. This is related to the Lode-angle as $\theta = \frac{1}{3}\sin^{-1}(K_3)$. By straightforward algebraic manipulations, the alternate third invariant can be written in terms of second and third invariants of the stress deviator as $K_3 = \frac{3\sqrt{3}J_3}{2J_2^{3/2}}$. We note that $-1 \leq K_3 \leq 1$ with $K_3 = -1$ for triaxial compression, $K_3 = 0$ for shear, and $K_3 = 1$ for triaxial extension. The Lode-angle varies as $-\frac{\pi}{6} \leq \theta \leq \frac{\pi}{6}$ with $\theta = -\frac{\pi}{6}$ for TXC, $\theta = 0$ for shear, and $\theta = \frac{\pi}{6}$ for TXE.

*e-mail: hharkira@caltech.edu

2.2 Yield criterion

In order to define the yield criterion, we adopt the functional form given in [15] as follows

$$f(\mathbf{T}) = \bar{\tau} \frac{\cos \left[\frac{\cos^{-1}(\beta_s K_3)}{3} - \gamma_s \frac{\pi}{6} \right]}{\cos \left[(1 - \gamma_s) \frac{\pi}{6} \right]} - \mu_s^0 p \quad (1)$$

where β_s and γ_s are dimensionless parameters, and $f(\mathbf{T}) = 0$ is the yield surface. Note that when $K_3 = 0$, the yield function simplifies to $f(\mathbf{T}) = \bar{\tau} - \mu_s^0 p$, such that for $f = 0$, the critical stress ratio $\mu = \frac{\bar{\tau}}{p} = \mu_s^0$, where μ_s^0 represents the yield value of μ for a pure shear state of stress ($K_3 = 0$). In this limit, the yield criterion reduces to the Drucker-Prager yield criterion which is same as the rate-independent limit of the original $\mu(I)$ form [8, 11, 16]. The other two notable stress states are triaxial extension $K_3 = 1$, and triaxial compression $K_3 = -1$. We will revisit these stress states and the associated yield criterion in detail in the subsequent discussion.

3 Fitting the yield threshold

The original local or $\mu(I)$ rheology [8, 11, 16] has two components: rate-independent critical stress ratio $\mu = \mu_s$ and the rate-dependent part capped by the stress ratio $\mu = \mu_2$. The relationship between the non-dimensional stress state μ and the non-dimensional strain-rate, the inertial number I , is given through a non-linear functional form [16] as follows

$$\mu = \mu_s + \frac{\mu_2 - \mu_s}{I_0/I + 1} \quad (2)$$

Thus, the local rheology has just three unknown parameters given as $\{\mu_s, I_0, \mu_2\}$. Typically, these parameters can be fitted to simple shear flows via discrete element simulations or to experimental data. However in reality, these parameters differ depending on the type of flow. For instance, it is a well known property [14] of geomaterials that they act stronger when subjected to the triaxial compression stress state than the triaxial extension stress state. In the subsequent discussion, we will study the dependence of these parameters on the flow type.

3.1 Rate-independent limit

Firstly, we study the yield criterion in the rate-independent limit. From eq. 1, $f(\mathbf{T}) = 0$ implies that the critical stress state associated with yield in the rate-independent limit can be written as follows

$$\mu_s(K_3) = \mu_s^0 \frac{\cos \left[(1 - \gamma_s) \frac{\pi}{6} \right]}{\cos \left[\frac{\cos^{-1}(\beta_s K_3)}{3} - \gamma_s \frac{\pi}{6} \right]}, \quad (3)$$

where μ_s^0 is the critical stress ratio in the case of a pure shear state of stress, and β_s and γ_s are the parameters dictating the shape of the yield surface as shown in fig. 1(a). Therefore, there are three unknown parameters in total for

the rate-independent part. In order to estimate these unknown parameters, we first look at the ratio $\mu_s^{\text{TXE}}/\mu_s^{\text{TXC}} = \mu_s(1)/\mu_s(-1)$ for a range of parameters $\{\beta_s, \gamma_s\}$ as shown in fig. 1(a). For most geomaterials, the ratio $\mu_s^{\text{TXE}}/\mu_s^{\text{TXC}}$ is less than 1. Therefore, the relevant range of parameters is $\beta_s \in (0, 1)$ and $\gamma_s \in (0, 1)$. We fit these two parameters to the μ_s/μ_s^{TXC} data from [14] and obtain $\{\beta_s = 0.58, \gamma_s = 0.26\}$. The fitted curve is shown by a black line in fig. 1(c), and the red solid circles are the data points from [14]. Finally, the remaining parameter μ_s^0 is fitted to the same but non-normalized $\mu_s(K_3)$ data as shown in fig. 1(d). The estimated value of the critical stress ratio in a pure shear state of stress is $\mu_s^0 = 0.33$. This way we completely characterize the yield criterion in the rate-independent limit.

3.2 Rate-dependence

Secondly, in order to account for the rate-dependence of the flow threshold, we invoke the nonlinear functional form of the local rheology given by eq. 2 and fit the two unknown parameters $\{I_0, \mu_2\}$ to rate-dependent triaxial extension and triaxial compression DEM data, reported in [14], as shown in fig. 2(a). The fitted value of μ_2 comes out different in the two cases, i.e., $\mu_2^{\text{TXE}} = 0.66$ and $\mu_2^{\text{TXC}} = 0.96$. This suggests that μ_2 also depends on the flow type or the third invariant K_3 . On the contrary, the fitted value of I_0 comes out close to 0.6 in the two aforementioned cases. For simplicity, we choose $I_0 = 0.6$ for all flow types, and ignore its dependence on the third invariant K_3 . We hypothesize that μ_2 depends on the flow type in the same manner as μ_s , and therefore, we assume following form

$$\mu_2(K_3) = \mu_2^0 \frac{\cos \left[(1 - \gamma_2) \frac{\pi}{6} \right]}{\cos \left[\frac{\cos^{-1}(\beta_2 K_3)}{3} - \gamma_2 \frac{\pi}{6} \right]}, \quad (4)$$

where μ_2^0 corresponds to the pure shear state of stress, and β_2 and γ_2 are fitting parameters. In the fitting procedure, we only consider the pairs of $\{\beta_2, \gamma_2\}$ such that the eq. 4 gives same value of $\mu_2^{\text{TXC}}/\mu_2^{\text{TXE}}$ as previously estimated in fig. 2(a). Further, we use the inverted form of local rheology as follows

$$I = \begin{cases} I_0 \frac{\mu - \mu_s(K_3)}{\mu_2(K_3) - \mu} & \text{if } \mu > \mu_s(K_3) \\ 0 & \text{if } \mu \leq \mu_s(K_3) \end{cases} \quad (5)$$

and fit the eq. 5 to the rate-dependent data from [14]. The fitted values of the unknowns come out as $\beta_2 = 0.82$, $\gamma_2 = 0$ and $\mu_2^0 = 0.74$. The fitted surface and the data from [14] are shown in fig. 2(b). This way we generalize the rate-dependent part of the rheology to account for its dependence on the flow types.

3.3 Yield surface

We use the modified $\mu(I, K_3)$ form to construct the yield surface, normalized by the hydrostatic pressure, in the π -plane. Specifically, we plot the two limits, $\mu_s(K_3)$

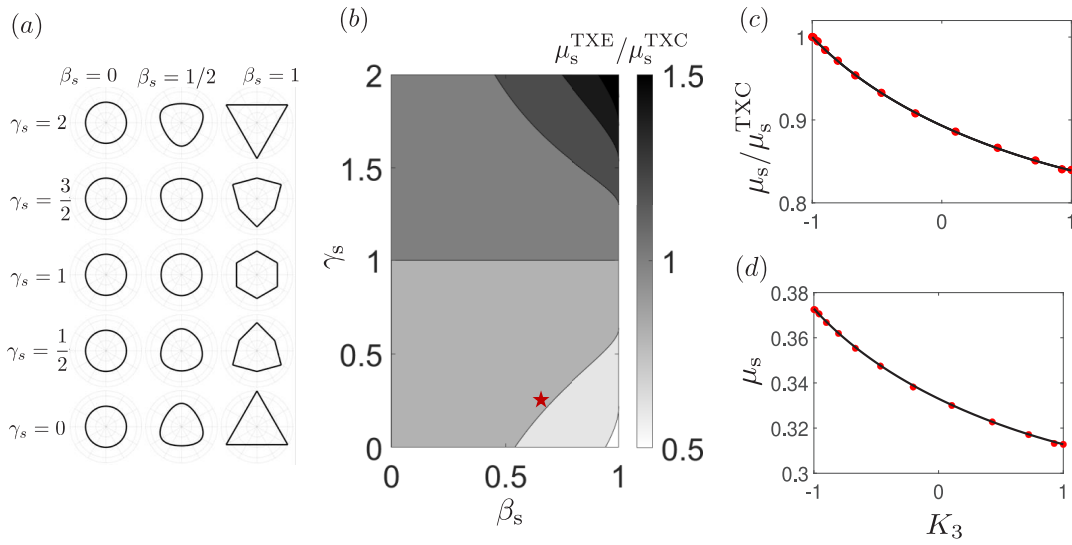


Figure 1. (a) Shape of the yield surface corresponding to different combinations of $\{\beta_s, \gamma_s\}$. (b) Contour representation of the ratio of the yield thresholds in triaxial extension and triaxial compression in the $\beta_s - \gamma_s$ parametric space. The red star depicts the fitted values of $\{\beta_s = 0.58, \gamma_s = 0.26\}$. The fitted $\mu_s^{\text{TXE}}/\mu_s^{\text{TXC}}$ and μ_s as a function of third invariant (K_3) are shown in (c) and (d), respectively. The red solid circles are the data points from [14].

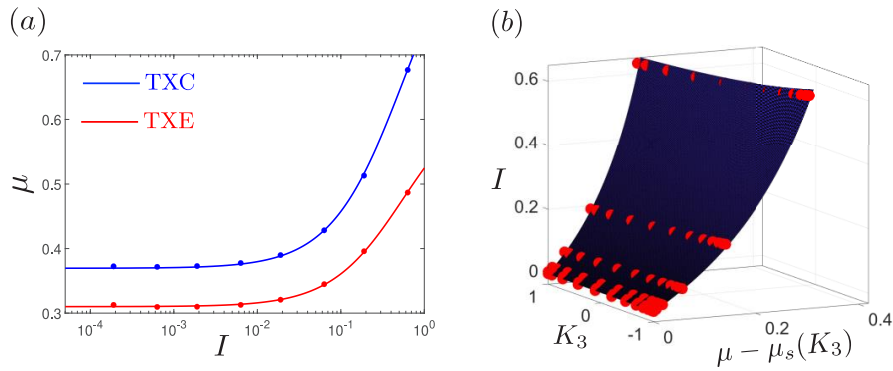


Figure 2. Depiction of the rate-dependent rheology for different flow types. (a) Fitting the $\mu(I)$ relation for the triaxial extension (TXE) and triaxial compression (TXC) cases. (b) The fitted $\mu(I)$ form as a function of third invariant (K_3). The red solid circles are the data points from [14]

and $\mu_2(K_3)$. The parameters associated with the rate-independent limit $\mu_s(K_3)$ are

$$\{\mu_s^0 = 0.33, \beta_s = 0.58, \gamma_s = 0.26\} \quad (6)$$

and the rate-dependent limit $\mu_2(K_3)$ are

$$\{\mu_2^0 = 0.74, \beta_2 = 0.82, \gamma_2 = 0\}. \quad (7)$$

We substitute the above parameters in eq. 3 and eq. 4 to construct the yield surface corresponding to the rate-independent limit given by $\mu_s(K_3)$ and the rate-dependent limit given by $\mu_2(K_3)$. The π -plane projections of the

yield surface are shown in fig. 3, where the black and red lines are used to represent the rate-independent and rate-dependent limits. The stress states corresponding to triaxial compression ($K_3 = -1$), pure shear ($K_3 = 0$) and triaxial extension ($K_3 = 1$) are highlighted in the plot. There are two interesting observations. First, in both limits, μ^{TXC} is greater than μ^{TXE} . Second, the shape of the yield surface is more rounded in the rate-independent limit and pointier in the rate-dependent limit, indicating that the dependence on flow type gets stronger with increasing I . In summary, we have constructed a generalized yield surface which ac-

counts for the mode of deformation in terms of K_3 as a function of the deformation rates.

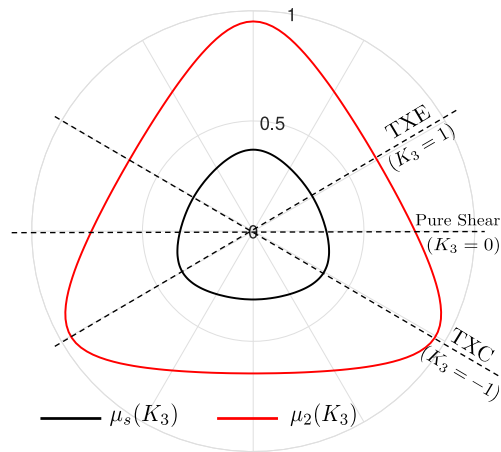


Figure 3. Depiction of flow threshold. The black line represents the yield surface μ_s , as a function of K_3 . The red line represents the yield surface μ_2 as a function of K_3 .

4 Conclusion

In this study, we propose a yield criterion that accounts for the different flow types ranging from triaxial compression to triaxial extension. The well-known local rheology, or the $\mu(I)$ rheology, is generalized by adapting the flow threshold, in the rate-independent and rate-dependent limits, to account for different flow types. The modified form of the $\mu(I)$ rheology is fitted to the extensive discrete element simulations carried out in [14]. It is noted that the yield threshold depends on the flow type, and the critical stress ratio in triaxial compression is greater compared to triaxial extension. In total, we introduce 7 parameters to fully generalize the $\mu(I)$ rheology, in contrast to 3 parameters in the original $\mu(I)$ form.

Generalization of local rheology is the first step in the direction of developing a non-codirectional flow rule that can account for peculiar behavior of dense granular flows such as normal stress differences and secondary or vortex-type flows. In the next step, it remains to formulate the direction of flow tensor and relate it to the stress tensor to construct the generalized flow rule. The flow rule can be used in the finite-element framework to simulate complex flow configurations which showcase normal stress differences [11] and secondary vortex flows [17]. These directions will be pursued in the future studies.

Acknowledgement: We gratefully acknowledge the financial support of the Office of Naval Research through MURI award N00014-23-1-2654.

References

[1] J. Gray, A. Thornton, A theory for particle size segregation in shallow granular free-surface flows, *Proc. Roy. Soc. London Ser. A* **461**, 1447 (2005).

[2] Y. Fan, K. Hill, Theory for shear-induced segregation of dense granular mixtures, *New Journal of Physics* **13**, 095009 (2011).

[3] A. Tripathi, D. Khakhar, Density difference-driven segregation in a dense granular flow, *J. Fluid Mech.* **717**, 643 (2013).

[4] H. Singh, D. Liu, D.L. Henann, Continuum modelling of size segregation and flow in dense, bidisperse granular media: accounting for segregation driven by both pressure gradients and shear-strain-rate gradients, *Journal of Fluid Mechanics* **988**, A43 (2024). [10.1017/jfm.2024.477](https://doi.org/10.1017/jfm.2024.477)

[5] H. Singh, D.L. Henann, Anti-plane segregation and diffusion in dense, bidisperse granular shear flow, *Phys. Rev. Fluids* **9**, 094301 (2024). [10.1103/PhysRevFluids.9.094301](https://doi.org/10.1103/PhysRevFluids.9.094301)

[6] T. Komatsu, S. Inagaki, N. Nakagawa, S. Nasuno, Creep motion in a granular pile exhibiting steady surface flow, *Phys. Rev. Lett.* **86**, 1757 (2001).

[7] G. MiDi, On dense granular flows, *Euro. Phys. Journ. E.* **14**, 341 (2004).

[8] P. Jop, Y. Forterre, O. Pouliquen, A constitutive law for dense granular flows, *Nature* **441**, 727 (2006).

[9] F. da Cruz, S. Emam, M. Prochnow, J. Roux, F. Chevoir, Rheophysics of dense granular materials: Discrete simulation of plane shear flows, *Phys. Rev. E.* **72**, 021309 (2005).

[10] K. Kamrin, Non-locality in granular flow: Phenomenology and modeling approaches, *Frontiers in Physics* **7**, 116 (2019).

[11] I. Srivastava, L. Silbert, G. Grest, J. Lechman, Viscometric flow of dense granular materials under controlled pressure and shear stress, *J. Fluid Mech.* **907**, A18 (2021).

[12] L. Staron, P.Y. Lagrée, S. Popinet, Continuum simulation of the discharge of the granular silo: A validation test for the $\mu(i)$ visco-plastic flow law, *Eur. Phys. J. E Soft Matter* **37**, 5 (2014).

[13] S. Dunatunga, K. Kamrin, Continuum modelling and simulation of granular flows through their many phases, *J. Fluid Mech.* **779**, 483 (2015).

[14] J.T. Clemmer, I. Srivastava, G.S. Grest, J.B. Lechman, Shear is not always simple: Rate-dependent effects of flow type on granular rheology, *Physical Review Letters* **127**, 268003 (2021).

[15] R. Lagioia, A. Panteghini, On the existence of a unique class of yield and failure criteria comprising tresca, von mises, drucker-prager, mohr-coulomb, galileo-rankine, matsuoaka-nakai and lade-duncan, *Proceedings of the royal society A: mathematical, physical and engineering sciences* **472**, 20150713 (2016).

[16] P. Jop, Y. Forterre, O. Pouliquen, Crucial role of side walls for granular surface flows: consequences for the rheology, *J. Fluid Mech.* **541**, 21 (2005).

[17] K.P. Krishnaraj, P.R. Nott, A dilation-driven vortex flow in sheared granular materials explains a rheometric anomaly, *Nat. Commun.* **7**, 10630 (2016).